nature climate change

ARTICLES

https://doi.org/10.1038/s41558-019-0583-9

Reduced resilience as an early warning signal of forest mortality

Yanlan Liu[1], Mukesh Kumar[1,2*], Gabriel G. Katul[1,3] and Amilcare Porporato[4,5]

Climate-induced forest mortality is being widely observed across the globe. Predicting forest mortality remains challenging because the physiological mechanisms causing mortality are not fully understood and empirical relations between climatology and mortality are subject to change. Here, we show that the temporal loss of resilience, a phenomenon often detected as a system approaches a tipping point, can be used as an early warning signal (EWS) to predict the likelihood of forest mortality directly from remotely sensed vegetation dynamics. We tested the proposed approach on data from Californian forests and found that the EWS can often be detected before reduced greenness, between 6 to 19 months before mortality. The EWS shows a species-specific relation with mortality, and is able to capture its spatio-temporal variations. These findings highlight the potential for such an EWS to predict forest mortality in the near-term.

Episodes of forest mortality have been widely observed in recent decades[1,2]. Such abrupt transitions in land cover impact local species composition and ecosystem services, as well as the global carbon balance[2,3]. Predictive approaches to climate-induced forest mortality are now proliferating either through modelling of plant physiological dynamics[4–6] or by inferring relations with hydroclimatic stresses[7–9]. However, given the complexity of mortality at the individual tree[10,11] and ecosystem levels[12,13], compounded by uncertainties in model structure and parameterization, predicting mortality using vegetation models alone remains challenging[14,15]. Relations between hydroclimatic stress and mortality provide another predictive approach[9,16], although its efficacy can be undermined by acclimation of vegetation properties and community competition. As these two approaches entail estimation of water and carbon budgets within the soil–plant system subject to projected climatic variability, uncertainties in these estimations are bound to influence the accuracy and uncertainty of mortality.

Here, we propose an alternative approach for predicting climate-induced forest mortality through the direct monitoring of vegetation dynamics. The resilience or the recovery rate from a deviated state is generally reduced near the tipping point where a shift in the system state occurs[17]. Here, the reduction in resilience can be caused by impaired physiological functions (Supplementary Fig. 1) that make the current forested state no longer stable or at least more vulnerable to transition under stochastic perturbations[18,19]. As a result, around the tipping point, the forest ecosystem can be nudged into a degraded dynamical regime such as one with a different forest composition or cover (for example, shrub land or grassy open area). These transitions can either be catastrophic or non-catastrophic depending on the configuration of the degraded state[20]. In either case, a consequence of reduced resilience or the critical slowing down near the tipping point is high temporal autocorrelation[17]. This property was leveraged in a recent study[21] to assess spatial patterns of static forest resilience. The idea of static resilience obtained for a given time period using autocorrelation can be extended to a dynamic metric to track temporal variations in resilience[22]. This study develops such a metric and evaluates the potential of using reduced resilience as an early warning signal (EWS) for impending climate-induced mortality. Here, an EWS is defined as abnormally low resilience measured by abnormally high lag-1 autocorrelation in vegetation dynamics (see Supplementary Notes for definitions of terms related to EWS).

Detecting an EWS

Previous studies[17,23,24] demonstrated the effectiveness of using an increased lag-1 temporal autocorrelation within a moving window as an EWS to abrupt changes. However, most of these studies were based on fully defined theoretical systems or control experiments and took advantage of sufficiently long time series. Application of this method in a 'real' ecosystem set-up is expected to be more challenging, in part due to the limited duration of the available time series, the presence of dominant seasonal frequencies in variations of both ecosystem response and forcing signals, variations in autocorrelation of the forcing signals and the presence of stochastic noise[24]. These challenges have partly contributed to the scarcity of examples detecting critical slowing down in real natural systems[22].

For these reasons, a Bayesian dynamic linear model (DLM) (see Methods and Supplementary Methods) is proposed. Similar to previous studies[25,26], the DLM uses a Kalman filter to evaluate time-varying autocorrelation. However, here the DLM also accounts for temporal variation of other components, including intrinsic stochastic noise, long-term trends and the seasonality inherent in both observed vegetation dynamics and climate forcings. Accounting for the variation in climate forcing can provide critical information for EWS detection[26] thereby improving its accuracy, especially by avoiding false alarms that arise from increasingly autocorrelated climate conditions (Supplementary Methods, Supplementary Fig. 5). Using the DLM and relevant climate data, the time-varying autocorrelation of normalized difference vegetation index (NDVI) was estimated for each 30 m pixel in Landsat 7 images for all forested areas in the state of California, USA, the study area. Mortality in the study area has been widely observed in recent years[27], with the potential

[1]Nicholas School of the Environment, Duke University, Durham, NC, USA. [2]Department of Civil, Construction, and Environmental Engineering, University of Alabama, Tuscaloosa, AL, USA. [3]Department of Civil and Environmental Engineering, Duke University, Durham, NC, USA. [4]Department of Civil and Environmental Engineering, Princeton University, Princeton, NJ, USA. [5]Princeton Environmental Institute, Princeton University, Princeton, NJ, USA. *e-mail: mkumar4@eng.ua.edu

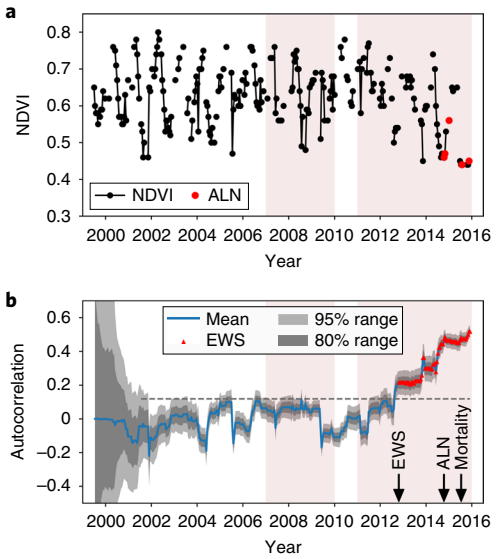

Fig. 1 | An example of EWS detected using the DLM. a, NDVI time series of a pixel in the southern Sierra **b**, Mean and uncertainty range of the time-varying autocorrelation estimated using the DLM. The EWS identified when the mean autocorrelation exceeds a threshold (grey dashed line) are shown, calculated as the long-term (excluding a two-year warm-up period) average of the upper boundary of the uncertainty range. Shaded time ranges indicate the two droughts according to the PDSI. The *x* axis values mark 1 January for each year.

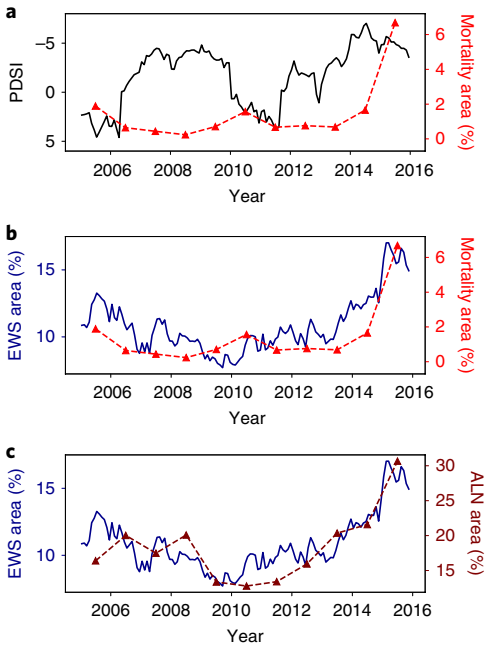

Fig. 2 | Temporal trajectories of drought severity, mortality area and EWS area from 2005 to 2015. a, Monthly PDSI values[31] for the state of California (black, left *y* axis) and the area with tree mortality (red, right *y* axis) from annual aerial surveys. **b**, Proportion of the area exhibiting EWS (blue, left *y* axis) and observed tree mortality (red, right *y* axis). **c**, Proportion of the area exhibiting EWS (blue, left *y* axis) and ALN (dark red, right *y* axis). The *x* axis values mark 1 January for each year.

to reduce the gross primary productivity both locally and across North America through eco-climate teleconnections[28]. A probability distribution of autocorrelation was obtained from the DLM at each time point during the period 1999–2015.On the basis of the estimated mean and uncertainty range of autocorrelation at each time point, the EWS was identified as the presence of a mean autocorrelation exceeding a threshold and lasting for at least 3 months. The threshold was computed as the long-term average of the 80th percentile of the estimated autocorrelation uncertainty range. The magnitude of this threshold, which is constant in time, provides a reference for defining the abnormal range of the EWS. An example application of the DLM on a pixel in the southern Sierra dominated by pines shows that the autocorrelation in NDVI time series became abnormally high, that is, exceeded the long-term average of its 80th percentile of the uncertainty range, after October 2012 (Fig. 1b). Abnormally low NDVI (ALN) that may indicate foliage shedding was identified in September 2014 (Fig. 1a) and eventual mortality was observed in July 2015. No mortality or fire was observed in the previous years. The presence of abnormally high autocorrelation, that is, reduced resilience, from October 2012 onwards serves as an EWS, with lead times of 23 months and 33 months to ALN and mortality, respectively, in this case. Although high autocorrelation is a typical signature of critical slowing down, it does not guarantee the occurrence of critical slowing down and an impending critical transition; that is, it is necessary but not sufficient. To further examine the representativeness of the EWS for critical slowing down, an independent analysis of NDVI data within the context of a nonlinear dynamic model of vegetation dynamics with two stable states was conducted. The two stable states in the model represent an existing vegetation cover and an alternative state[19]. The analysis suggests that during the period when an EWS was identified, the system slowed down and the basin of attraction shrank (Supplementary Discussion, Supplementary Fig. 15). These shifts represent reduced recovery rate and a higher likelihood of a switch to an alternative state under stochastic perturbations. The occurrence of critical slowing down in the NDVI data during the EWS period within this model provides additional support for using the empirically derived EWS to predict state transitions.

The DLM was applied to the rest of the pixels in the study area to identify EWS. Temporal and spatial variations in the detected EWS were compared with aerially observed mortality provided by the US Forest Service each year since 2005[27]. Mortality noted as caused by fire or human activities was excluded from the analyses. As the forest mortality map from the aerial surveys delineates geospatial polygons within which some, rather than all, of the trees died, whereas the EWS provides a pixel-based estimate at a 30 m resolution, the comparison may introduce errors due to the mismatch in spatial scales. A comparison of the EWS was also performed against an incidence map of ALN, which has the same resolution as EWS and could be associated with leaf shedding or vegetation die-off[29,30]. Hereafter, ALN represents the occurrence of NDVI values lower than a threshold, lasting for at least half of the time in the following 3 months. This threshold is set equal to the lower 20th percentile of all of the observed NDVI values in that month at a given pixel location. The sensitivity analysis indicates that the conclusions are robust with respect to the chosen thresholds (Supplementary Discussion, Supplementary Figs. 20–24, Supplementary Table 3).

Fraction of the area showing EWS

During 2005–2015, the Palmer drought severity index (PDSI)[31] indicated that the state of California underwent two major droughts spanning 2007–2009 and 2012–2015 (Fig. 2a). For the entire study area, the fraction of the area with observed mortality intensity greater than one tree per acre[27], that is, mortality area, remained below 2% during the first drought but rapidly increased to 6.7% in 2015 (Fig. 2a). This sharp increase in mortality area during the second drought was in contrast to the temporal variation in PDSI vales, which gradually increased during 2012–2014 and remained

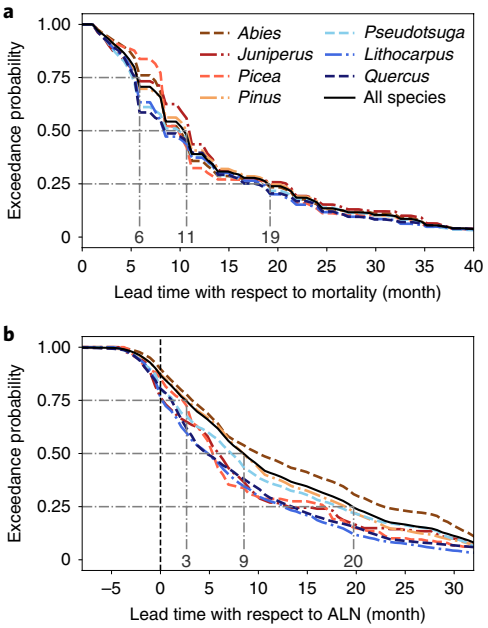

Fig. 3 | Exceedance probability of the lead time of the EWS. a,**b**, Lead times with respect to mortality (**a**) and ALN (**b**). Black solid lines in both plots represent the entire surveyed area; coloured dashed lines represent the areas dominated by the major species listed, each of which covers an area greater than 1,000 km^2. The legend applies to both plots.

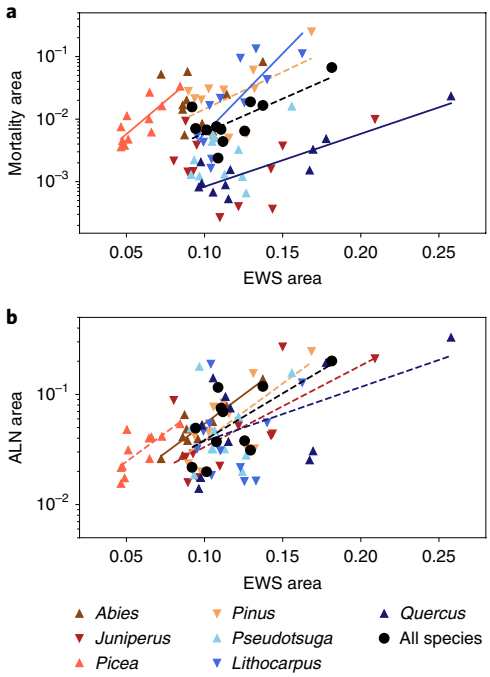

Fig. 4 | Species-specific relations of the area showing EWS with mortality during the period 2005–2015. a,**b**, The proportion of the areas showing EWS that experienced mortality (**a**) and ALN (**b**). Each triangle represents one major species (see legend) and black dots all species in each year. Solid trend lines denote a significance level of $P < 0.01$ and dashed trend lines denote a significance level of $P < 0.05$. Trend lines are not plotted for species without significant relations.

high afterwards. The temporal pattern of mortality follows a typical signature of critical transitions of ecosystems under slowly varying environmental drivers[24]. The fraction of the area showing an EWS exhibited similar temporal variation, with the areal fraction remaining around 10% during the first drought but then increasing to a high value of 16% by 2015 (Fig. 2b). The computed EWS area was generally larger than the mortality area, indicating that some trees operated under low resilience without loss of life. The extent of the area exhibiting EWS and ALN (Fig. 2c) depends on the thresholds used to identify these metrics (Supplementary Discussion, Supplementary Fig. 20). However, all of the thresholds considered result in temporal trajectories of the area exhibiting EWS that follow a similar pattern to ALN and mortality. Such prominent temporal correspondence highlights the potential of using low resilience (high autocorrelation) as an EWS to track interannual variations in forest mortality.

Lead time of the EWS

For areas where the EWS was detected before the observed mortality, 75% of the cases exhibited EWS more than 6 months before mortality; 25% of the cases showed EWS more than 19 months before mortality (Fig. 3a). When compared with detected ALN (Fig. 3b), the EWS was identified earlier in 87% of the cases and 9 months earlier in 50% of the cases, highlighting the advantage of the resilience-based EWS over the drop in greenness in predicting mortality. Among differing species, the lead time of the EWS exhibited little difference with respect to mortality (Fig. 3a), but a larger difference with respect to ALN (Fig. 3b). For example, *Juniperus* (juniper) and *Quercus* (oak) experienced ALN much sooner after the first occurrence of the EWS than *Abies* (fir) and *Pinus* (pine), possibly due to their higher tendency to drop leaves under stress[32,33].

Spatio-temporal estimation and prediction

Throughout the entire study area, mortality area and ALN area in each year were positively correlated with EWS area ($P < 0.05$) (Fig. 4a,b, black dots). However, they did not exhibit an apparent relation to the duration of the EWS (Supplementary Discussion, Supplementary Fig. 16). The relation between EWS area and mortality area differed among the seven dominant species in the study area (Fig. 4a,b, coloured triangles). For example, for *Quercus*, *Lithocarpus* (tanoak), *Pinus* and *Picea* (spruce), 10% of the EWS area corresponded to 0.1%, 0.6%, 1.4% and 6.5% of mortality area, respectively. These differences imply that oaks are more likely to survive under low resilience than spruces and pines. The result is consistent with previous studies conducted in the western United States, where isohydric species such as pines and spruces that are susceptible to stomatal closure under stress were found to succumb at a higher frequency during prolonged drought, possibly due to carbon starvation[34,35]. In contrast, anisohydric species such as junipers and oaks that adopt a more aggressive water-use strategy experienced less mortality, partly because of the smaller likelihood of stomatal closure and advantages arising from adjustments of fine root density and leaf area[35,36]. Notably, the correlations between EWS area and mortality area vanished when all species were aggregated, even when they were located in the same eco-climate region (Supplementary Discussion, Supplementary Fig. 17). This distinction suggests that resilience signatures are more species dependent than eco-climate condition dependent, which could result from distinct species-specific traits[15]. The direct implication is that species distribution information is necessary when translating detected EWS into mortality area.

Temporally, with a zero lead time (at the same time point when mortality was observed), 96% of the interannual variation in mortality area for the entire study area was explained using species-specific quadratic functions of EWS area (Fig. 5). When using EWS area detected 3, 6, 9 and 12 months earlier than observed mortality, the estimation accuracy gradually decreased to 91%, 77%, 33% and 41% respectively (Fig. 5, blue solid line). The leave-one-out

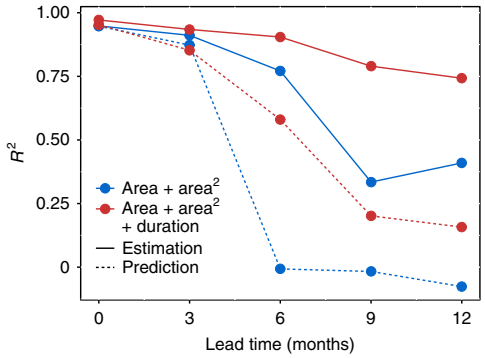

Fig. 5 | Temporal estimation and prediction accuracies using EWS characteristics with lead times ranging from 0 to 12 months. Blue and red lines denote accuracies using EWS area only and using both EWS area and duration, respectively. The EWS area was represented using a linear and a quadratic term, whereas the duration was represented using a linear term. Estimation accuracies (solid lines) were computed using the regression relation obtained based on data for all years, while prediction accuracies (dashed lines) were obtained using a leave-one-out cross validation strategy.

prediction accuracy dropped to around zero with longer lead times (≥6 months, Fig. 5, dashed blue line). The accuracy was improved by the addition of a linear EWS duration term, but was not improved further by additional quadratic or interaction terms (Supplementary Discussion, Supplementary Fig. 18).

The estimation accuracy of mortality was analysed at multiple spatial scales, ranging from the eco-climate region to 1/2°, 1/8° and 3 km. In addition to the previously studied variables of topography[37] and community competition[16], which are known to influence the spatial pattern of mortality, the contribution of the EWS area and duration were also found to be crucial based on the Bayesian Information Criterion (Supplementary Discussion, Supplementary Table 2). For years from 2005 to 2015, at a spatial resolution of 1/8° and with a 6 month lead time, the selected variables led to estimation accuracies of 0.89–0.93, areas under the receiver operating characteristic curve (AUC) of 0.61–0.71 for mortality occurrence and coefficients of determination (R^2) of 0.41–0.59 for mortality intensity. The estimation performance decreases at finer spatial scales (Supplementary Discussion, Supplementary Fig. 19). For example, 69%, 57%, 53% and 47% of the spatial variation in mortality intensity can be explained at eco-climate region, 1/2°, 1/8° and 3 km spatial scales, respectively, for the median year. It is worth noting that compared with mortality observed in 2009 (Fig. 6a) and 2015 (Fig. 6d) drought years at a 1/8° resolution, EWS characteristics together with information on topography and community competition can capture the spatial gradient of mortality within each year (Fig. 6b,e), and the overall higher mortality intensity in 2015. Spatial prediction using EWS detected 6 months ahead of observation showed that the overall spatial gradient and differences between the two drought years were ably captured (Fig. 6c, f). However, mortality rates were higher than predicted in the southern Sierra and the northeast of the study area in 2015 (Fig. 6d).

Discussion

A new approach for detecting a low-resilience-based EWS is proposed. The lead time of the EWS and its ability to estimate and predict forest mortality are examined. Given that the EWS relies on the physical phenomenon of critical slowing down near a tipping point, its detection is made possible by integrating a theoretical basis of the resilience of nonlinear dynamical systems approaching a tipping point[17], a statistical technique for inferring time-varying autocorrelation[38] and ever-proliferating, high-spatial-resolution remote sensing images of NDVI. The tipping point here is forest mortality due to drought.

The reduction in resilience before climate-induced mortality can be viewed through the lens of the physiological response of vegetation under stress. During drought, heat stress and water deficits deplete plant water content[30], induce malfunction of plant hydraulic systems due to cavitation spread, and restrict carbon uptake and transport via stomatal closure[10]. These stresses could further limit the capability of plants to refill cavitated xylem and replenish carbon storage to support metabolism and growth[11], thus handicapping recoverability from drought. The impact of the aforementioned stressors can be expressed as a slowed recovery rate of photosynthetic capability and foliage biomass, which can be captured in NDVI dynamics[39]. As this derived dynamic metric allows the detection of low resilience directly from NDVI time series, it circumvents the uncertainties inherent in mortality predictions based on climate stress metrics alone. Furthermore, the EWS provides predictability without relying on the prediction of climate conditions due to its dependence on increased autocorrelation.

While the results demonstrate the potential of the EWS to capture the spatio-temporal variations in ALN and mortality over a range of parameters used to detect the EWS and across both snow-affected and snow-free regions (Supplementary Discussion, Supplementary Figs. 20–29), two major challenges remain. The first is the representativeness of the identified resilience signal based on autocorrelation of NDVI values, which can be impaired by missing data on cloudy and snow days, and the uncertainties inherent in NDVI data, such as those due to measurement error, varying atmospheric composition over time and mixed signals from understory species. The effectiveness of EWS may also be affected by autocorrelation signatures in latent driving factors other than the considered climate conditions, such as local nutrient availability and biotic interactions with microbes and insects. In addition, as the relationship between the EWS and mortality is found to be species-specific, uncertainties in the species distribution map and the coexistence of multiple species may impair the accuracy of the EWS. Second, and perhaps more important, is the influence of stochastic perturbations on vegetation stress within the lead time and across space. While low resilience indicates a higher probability of state transition for given stochastic perturbations, the likelihood of mortality may be enhanced (reduced) if climate conditions are more unfavourable (favourable) during the lead time. Such uncertainty of climate variations increases with lead time, which explains lower prediction accuracies when using the EWS for longer lead times (Fig. 5). Similarly, mortality may also intensify at locations with moderate resilience due to localized insect/pathogen attack, which is in fact noted as the major causal agent of damage for 83% of forest mortality in the study area[27]. Such outbreaks are strongly influenced by climate-induced stresses, as the limited carbon uptake and transport during periods of drought restrict resin production, which is known to be a major defence agent against biotic attack[10,14,40]. The increase in plant susceptibility further promotes insect/pathogen populations[33]. While these perturbations reduce the prediction accuracy of the EWS for mortality (especially at fine resolutions), given their general dependence on climate-induced stresses, this influence is smoothed out at coarser scales, resulting in a robust relation between low resilience and mortality.

EWS detection in this study benefits from the incorporation of knowledge of the dynamical system embedded in the structure of the DLM, including interannual variations, seasonal cycles and impacts of climate forcings, while using noise as a substitute for other unknown dynamics. Future work may investigate the role of other variables that are currently lumped as noise on forest resilience. Variables with large contributions, as quantified by the model likelihood, can be included in the DLM. Note that the

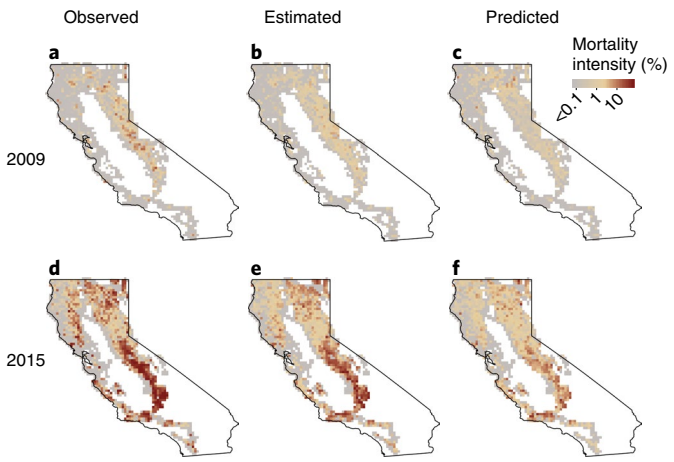

Fig. 6 | Observed, estimated and predicted mortality intensity in 2009 and 2015. a–f, The observed (**a**,**d**), estimated (**b**,**e**) and predicted (**c**,**f**) mortality intensity in 2009 (**a–c**) and 2015 (**d–f**). Estimations were conducted using the EWS detected with a zero lead time, and predictions were conducted using EWS detected 6 months ahead. Both the estimated and predicted mortality intensity were computed using a Gaussian process model that incorporates predictors of EWS characteristics, elevation, basal area and a spatial correlation structure.

NDVI-based EWS used in this study represents one aspect of forest dynamics—that is, the stress-induced change in resilience. Several other aspects of forest dynamics have recently been assessed to differentiate mortality and survival, including radial growth rate[41,42] from tree ring data, the fraction of non-photosynthetically active vegetation[43], the long-term trend and abrupt jumps in vegetation indices from remote sensing[44]. Future studies may focus on the intercomparison and fusion of the aforementioned metrics, or use new state variables and vegetation indices to develop effective representations of the state and stability of forest. In addition, to improve mortality prediction, especially with long lead times and at fine spatial scales, future efforts may seek to combine the EWS with predicted climate conditions, hydrological states, and knowledge of insect/pathogen habitation and mechanisms of infestation initiation and propagation during the lead time. EWS-based predictions could also benefit from better quantification of the thresholds used to detect the EWS and from more accurate data of forest properties. It is worth noting that the lead time of the EWS with respect to ALN and mortality mostly lies within two years (Fig. 3), similar to the timescale of recovery from drought[45]. Such consistency in timescales implies comparable probabilities of reaching full recovery or mortality starting from a stressed state. Further inquiry into the physiological controls on low resilience and their evolution towards eventual recovery or mortality for different species is necessary. Investigation in this regard may involve a comparison of the low-resilience signal with observed physiological metrics across scales[30,46].

Despite the aforementioned challenges, the results point towards significant opportunities ahead, given the apparent spatial and temporal associations between the detected EWS and actual mortality. The lead time of the EWS will allow forest managers to assess resource risks, and possibly prescribe approaches to mitigate insect and fire risks and restore stand health through prescribed burning, variable density thinning, and altering age structure and species composition[47,48]. The presented framework could be tested and applied to live monitoring of forest health under drought[49], and near-term prediction of climate-induced mortality in other forested regions of the world.

Online content

Any methods, additional references, Nature Research reporting summaries, source data, statements of code and data availability and associated accession codes are available at https://doi.org/10.1038/s41558-019-0583-9.

Received: 10 January 2019; Accepted: 22 August 2019;
Published online: 07 October 2019

References

1. Van Mantgem, P. J. et al. Widespread increase of tree mortality rates in the western United States. *Science* **323**, 521–524 (2009).
2. Allen, C. D. et al. A global overview of drought and heat-induced tree mortality reveals emerging climate change risks for forests. *For. Ecol. Manage.* **259**, 660–684 (2010).
3. Settele, J. et al. in *Climate Change 2014: Impacts, Adaptation, and Vulnerability* (eds Field, C. B. et al.) 271–359 (IPCC, Cambridge Univ. Press, 2015).
4. McDowell, N. G. et al. Evaluating theories of drought-induced vegetation mortality using a multimodel-experiment framework. *New Phytol.* **200**, 304–321 (2013).
5. Parolari, A. J., Katul, G. G. & Porporato, A. An ecohydrological perspective on drought-induced forest mortality. *J. Geophys. Res. Biogeosci.* **119**, 965–981 (2014).
6. Liu, Y. et al. Increasing atmospheric humidity and CO_2 concentration alleviate forest mortality risk. *Proc. Natl Acad. Sci. USA* **114**, 9918–9923 (2017).
7. Adams, H. D. et al. Temperature sensitivity of drought-induced tree mortality portends increased regional die-off under global-change-type drought. *Proc. Natl Acad. Sci. USA* **106**, 7063–7066 (2009).
8. Anderegg, L. D. L., Anderegg, W. R. L., Abatzoglou, J., Hausladen, A. M. & Berry, J. A. Drought characteristics' role in widespread aspen forest mortality across Colorado, USA. *Glob. Change Biol.* **19**, 1526–1537 (2013).
9. Anderegg, W. R. et al. Tree mortality predicted from drought-induced vascular damage. *Nat. Geosci.* **8**, 367–371 (2015).
10. McDowell, N. G. Mechanisms linking drought, hydraulics, carbon metabolism, and vegetation mortality. *Plant Physiol.* **155**, 1051–1059 (2011).
11. McDowell, N. G. et al. The interdependence of mechanisms underlying climate-driven vegetation mortality. *Trends Ecol. Evol.* **26**, 523–532 (2011).
12. Clark, J. S. et al. The impacts of increasing drought on forest dynamics, structure, and biodiversity in the United States. *Glob. Change Biol.* **22**, 2329–2352 (2016).
13. Wolf, A., Anderegg, W. R. & Pacala, S. W. Optimal stomatal behavior with competition for water and risk of hydraulic impairment. *Proc. Natl Acad. Sci. USA* **113**, E7222–E7230 (2016).
14. Sala, A., Piper, F. & Hoch, G. Physiological mechanisms of drought-induced tree mortality are far from being resolved. *New Phytol.* **186**, 274–281 (2010).
15. Choat, B. et al. Triggers of tree mortality under drought. *Nature* **558**, 531–539 (2018).
16. Young, D. J. et al. Long-term climate and competition explain forest mortality patterns under extreme drought. *Ecol. Lett.* **20**, 78–86 (2017).
17. Scheffer, M. et al. Early-warning signals for critical transitions. *Nature* **461**, 53–59 (2009).
18. van Nes, E. H. et al. What do you mean, 'tipping point'? *Trends Ecol. Evol.* **31**, 902–904 (2016).
19. Scheffer, M., Carpenter, S., Foley, J. A., Folke, C. & Walker, B. Catastrophic shifts in ecosystems. *Nature* **413**, 591–596 (2001).
20. Kéfi, S., Dakos, V., Scheffer, M., Van Nes, E. H. & Rietkerk, M. Early warning signals also precede non-catastrophic transitions. *Oikos* **122**, 641–648 (2013).
21. Verbesselt, J. et al. Remotely sensed resilience of tropical forests. *Nat. Clim. Change* **6**, 1028–1031 (2016).
22. Scheffer, M., Carpenter, S. R., Dakos, V. & van Nes, E. H. Generic indicators of ecological resilience: inferring the chance of a critical transition. *Annu. Rev. Ecol. Evol. Syst.* **46**, 145–167 (2015).
23. Dakos, V. et al. Slowing down as an early warning signal for abrupt climate change. *Proc. Natl Acad. Sci. USA* **105**, 14308–14312 (2008).
24. Dakos, V., Carpenter, S. R., van Nes, E. H. & Scheffer, M. Resilience indicators: prospects and limitations for early warnings of regime shifts. *Phil. Trans. R. Soc. B* **370**, 20130263 (2015).
25. Ives, A. R. & Dakos, V. Detecting dynamical changes in nonlinear time series using locally linear state-space models. *Ecosphere* **3**, 1–15 (2012).
26. Dakos, V. et al. Methods for detecting early warnings of critical transitions in time series illustrated using simulated ecological data. *PLoS ONE* **7**, e41010 (2012).
27. *US Forest Service Pacific Southwest Region Forest Health Protection Aerial Detection Survey* (US Forest Service, accessed 25 September 2017); https://www.fs.usda.gov/detail/r5/forest-grasslandhealth

28. Swann, A. L. et al. Continental-scale consequences of tree die-offs in North America: identifying where forest loss matters most. *Environ. Res. Lett.* **13**, 055014 (2018).
29. Breshears, D. D. et al. Regional vegetation die-off in response to global-change-type drought. *Proc. Natl Acad. Sci. USA* **102**, 15144–15148 (2005).
30. Brodrick, P. & Asner, G. Remotely sensed predictors of conifer tree mortality during severe drought. *Environ. Res. Lett.* **12**, 115013 (2017).
31. Dai, A., Trenberth, K. E. & Qian, T. A global dataset of Palmer drought severity index for 1870–2002: relationship with soil moisture and effects of surface warming. *J. Hydrometeorol.* **5**, 1117–1130 (2004).
32. Limousin, J.-M. et al. Morphological and phenological shoot plasticity in a Mediterranean evergreen oak facing long-term increased drought. *Oecologia* **169**, 565–577 (2012).
33. Gaylord, M. L. et al. Drought predisposes piñon-juniper woodlands to insect attacks and mortality. *New Phytol.* **198**, 567–578 (2013).
34. Mueller, R. C. et al. Differential tree mortality in response to severe drought: evidence for long-term vegetation shifts. *J. Ecol.* **93**, 1085–1093 (2005).
35. McDowell, N. et al. Mechanisms of plant survival and mortality during drought: why do some plants survive while others succumb to drought? *New Phytol.* **178**, 719–739 (2008).
36. Munné-Bosch, S. & Alegre, L. Die and let live: leaf senescence contributes to plant survival under drought stress. *Funct. Plant Biol.* **31**, 203–216 (2004).
37. Tai, X., Mackay, D. S., Anderegg, W. R., Sperry, J. S. & Brooks, P. D. Plant hydraulics improves and topography mediates prediction of aspen mortality in southwestern USA. *New Phytol.* **213**, 113–127 (2017).
38. Prado, R. & West, M. *Time Series: Modeling, Computation, and Inference* (CRC, 2010).
39. Vicente-Serrano, S. M. et al. Response of vegetation to drought time-scales across global land biomes. *Proc. Natl Acad. Sci. USA* **110**, 52–57 (2013).
40. Novick, K., Katul, G., McCarthy, H. & Oren, R. Increased resin flow in mature pine trees growing under elevated CO_2 and moderate soil fertility. *Tree Physiol.* **32**, 752–763 (2012).
41. Camarero, J. J., Gazol, A., Sangüesa-Barreda, G., Oliva, J. & Vicente-Serrano, S. M. To die or not to die: early warnings of tree dieback in response to a severe drought. *J. Ecol.* **103**, 44–57 (2015).
42. Cailleret, M. et al. A synthesis of radial growth patterns preceding tree mortality. *Glob. Change Biol.* **23**, 1675–1690 (2017).
43. Anderegg, W. R., Anderegg, L. D. & Huang, C.-y Testing early warning metrics for drought-induced tree physiological stress and mortality. *Glob. Change Biol.* **25**, 2459–2469 (2019).
44. Rogers, B. M. et al. Detecting early warning signals of tree mortality in boreal North America using multiscale satellite data. *Glob. Change Biol.* **24**, 2284–2304 (2018).
45. Schwalm, C. R. et al. Global patterns of drought recovery. *Nature* **548**, 202–205 (2017).
46. Walther, S. et al. Satellite chlorophyll fluorescence measurements reveal large-scale decoupling of photosynthesis and greenness dynamics in boreal evergreen forests. *Glob. Change Biol.* **22**, 2979–2996 (2016).
47. Churchill, D. J. et al. Restoring forest resilience: from reference spatial patterns to silvicultural prescriptions and monitoring. *For. Ecol. Manage.* **291**, 442–457 (2013).
48. Hessburg, P. F. et al. Tamm review: management of mixed-severity fire regime forests in Oregon, Washington, and Northern California. *For. Ecol. Manage.* **366**, 221–250 (2016).
49. Trumbore, S., Brando, P. & Hartmann, H. Forest health and global change. *Science* **349**, 814–818 (2015).

Acknowledgements

We thank J.S. Clark, M. West and C. Rundel for discussions and insightful suggestions. M.K. acknowledges support from the National Science Foundation (NSF, grant nos. EAR-1454983 and EAR-1331846). G.K. acknowledges support from the NSF (grant nos. EAR-1344703, AGS-1644382, IOS-1754893 and DGE-1068871). A.P. acknowledges support from the NSF (grant nos. EAR-1331846, DGE-1068871 and EAR-1316258). The publication cost was shared by The University of Alabama–Alabama Water Institute.

Author contributions

Y.L. and M.K. conceived the study. Y.L. prepared data and performed the analysis. G.K. and A.P. further improved the physical basis and assumptions. All authors contributed to interpreting the results and writing the manuscript.

Competing interests

The authors declare no competing interests.

Additional information

Supplementary information is available for this paper at https://doi.org/10.1038/s41558-019-0583-9.

Correspondence and requests for materials should be addressed to M.K.

Peer review information *Nature Climate Change* thanks Christopher Schwalm and the other, anonymous, reviewer(s) for their contribution to the peer review of this work.

Reprints and permissions information is available at www.nature.com/reprints.

Publisher's note Springer Nature remains neutral with regard to jurisdictional claims in published maps and institutional affiliations.

Methods

Vegetation and climate data. The United States Forest Service conducts annual aerial surveys over the forested area in California, providing maps that consist of polygons delineating the areas with aerially observed mortality[27]. The observed mortality maps from 2005 to 2015 were re-projected and rasterized at 30 m resolution to match with remotely sensed NDVI data. Regions with a mortality intensity greater than 1 tree per acre based on the aerial survey data were used for analysis. Landsat 7 ETM+ surface reflectance product[50] from June 1999 to December 2015 with a spatial resolution of 30 m and a temporal interval of 16 days was used to compute NDVI in the study area. Owing to the large amount of the original Landsat data, NDVI was computed and exported in tiles from Google Earth Engine. All the pixels in California with non-zero canopy closure for vegetation taller than 5 m were included in the study area on the basis of the 30 m resolution map of tree cover in 2000[51]. Areas with mortality caused by human activities, as indicated in the aerial survey maps, were excluded from analysis. Pixels affected by fire each year were identified based on the MODIS Active Fire product[52] and removed from estimation and prediction analysis. Data on cloudy or snow cover days were removed based on the 'cfmask' band, and were considered as missing data in DLM (Supplementary Methods, Supplementary Equations (4)–(6)). Climate conditions for daily precipitation, snow water equivalent, air temperature, incident shortwave radiation and water vapour pressure were obtained from Daymet V3[53]. These daily climate conditions at 1 km spatial resolution were downscaled and averaged over the 16 days between two satellite observations to achieve consistent spatial and temporal resolutions with NDVI. Covariates of elevation[54] and live basal area[55] that quantify topography[37] and community competition[16] were also rescaled to uniform scales for spatial estimation and prediction. The vegetation species distribution derived from field surveys during 1997–2014[56] was grouped to a genus level. The spatial distributions of dominant species covering an area greater than 1,000 km^2 were used to develop species-specific relations between EWS and observed forest mortality and ALN.

Bayesian DLM. The Bayesian DLM consists of an observation equation and a state evolution equation; that is:

$$y_t = \mathbf{F}_t^T \boldsymbol{\theta}_t + v_t \quad (1)$$

$$\boldsymbol{\theta}_t = G\,\boldsymbol{\theta}_{t-1} + \mathbf{w}_t \quad (2)$$

where y_t is the observed variable (NDVI) at time t after subtracting the long-term mean; $\mathbf{F}_t$ is a p-dimensional vector of known constants or regressors at time t, including climate variables and NDVI at time $t-1$; $\boldsymbol{\theta}_t$ is a p-dimensional state vector at time t, containing coefficients representing local mean, trend, seasonality, sensitivity to climate conditions and the lag-1 autocorrelation of NDVI; v_t is the observation noise following a zero mean Gaussian distribution; G is a known $p \times p$ state evolution matrix considered to be time-invariant; $\mathbf{w}_t$ is the state evolution noise at time t following a mean zero multivariate Gaussian distribution, and is independent of v_t. Non-informative priors for $\boldsymbol{\theta}_0$ and noises were provided (Supplementary Methods). At each time t, using forward filtering[38,57], the posterior distribution of $\boldsymbol{\theta}_t$ was estimated by combining the prior from the summary of history ($y_0, y_1, \ldots, y_{t-1}$) and the likelihood from current observation of y_t, resulting in a time-varying posterior distribution of $\boldsymbol{\theta}_t$. Of particular interest is the temporal trajectory of the entry in $\boldsymbol{\theta}_t$ quantifying the relation between y_t and y_{t-1}. This lag-1 autocorrelation was used as a time-varying measure of resilience. The EWS was then identified as the presence of this autocorrelation at a higher value than a threshold (Fig. 1). Theoretical details and controlled synthetic experiments demonstrating the efficacy of the DLM can be found in the Supplementary Methods. The source code of the DLM is available at https://github.com/YanlanLiu/early-warning-signal-DLM.

Spatio-temporal estimation and prediction. Temporally, the total fraction of the area showing the EWS and the average EWS duration for each species within the entire study area were used to explain and predict mortality area across years. For the years 2005–2015, all pixels in the study area except those affected by fire within three years were aggregated to assess the R^2 value of the temporal estimation. For prediction, one of the 11 years was left out each time and then predicted on the basis of the relations developed using the rest of the years. The accuracy was then computed by comparing the predictions with the observations. Estimation and prediction accuracies obtained using different combinations of EWS characteristics and lead times were examined (Fig. 5, Supplementary Fig. 18). Spatially, as the mortality area is highly zero-inflated, mortality occurrence (that is, whether the mortality area is greater than 0.1%) and mortality intensity (that is, the magnitude of the mortality area for pixels with mortality occurrence) were modelled separately using a Gaussian model and a binomial model, respectively. The analyses were conducted at spatial resolutions of 3 km, 1/8 degree, 1/2 degree, and eco-climate region. Candidate predictors include the fraction of the area showing the EWS, EWS duration, basal area and elevation in each pixel. Among the linear, quadratic and interaction terms of these predictors, the most informative predictors were selected on the basis of the Bayesian Information Criterion for each species (Supplementary Table 2). Apart from the selected predictors, a spatial Gaussian process was also incorporated to describe the spatial similarity among close neighbours. The point-based Gaussian process model is expressed as follows.

$$y(\mathbf{s}) = \mathbf{x}^T \boldsymbol{\beta} + w(\mathbf{s}) + \sigma \quad (3)$$

where $y(\mathbf{s})$ is mortality intensity at location $\mathbf{s}$ in the Gaussian model and the logit of mortality occurrence probability in the binomial model; $\mathbf{x}$ is a vector containing the selected predictors at location $\mathbf{s}$ and $\boldsymbol{\beta}$ contains the corresponding coefficients; $w(\mathbf{s})$ is the spatial effect of a Gaussian process with an exponential covariance function; and σ is the residual. Owing to the distinct relationship between the EWS and mortality area among species (Fig. 4), this spatial model was fitted for each of the dominant species separately. For the spatial estimation, the model was fitted for mortality occurrence and log-transformed intensity in each year using the functions spGLM and spLM, respectively, in the spBayes software[58] in R[59]. A non-informative flat prior was used for $\boldsymbol{\beta}$; and priors for $w(\mathbf{s})$ were obtained from empirical variogram. Estimates were computed using posterior means of $\boldsymbol{\beta}$ and $w(\mathbf{s})$ from 10^4 Markov chain Monte Carlo samples after a 2,000-sample burn-in period. For the spatial prediction, $\boldsymbol{\beta}$ was set as the coefficient of linear regression obtained using pixels dominated by a given species from all years; $\boldsymbol{\beta}$ was kept the same for all years for consistency in the accuracy evaluation. For operational purposes, all historical data should be used in the estimation, for which the representativeness is expected to improve as the number of samples increases. The spatial structure $w(\mathbf{s})$ was considered as a random walk from that of the previous year[60], with the mean spatial surface unchanged. In this way, the spatial distribution of mortality occurrence and intensity in a given year can be predicted using only historical data; that is, predictors observed at a given lead time and the mean spatial structure from the most recent year. Spatial accuracies for mortality occurrence in each year were assessed using the overall accuracy and the area under the receiver operating characteristic curve metrics (see Supplementary Discussion); accuracies for mortality intensity were assessed using the Bayesian R^2[61].

Reporting Summary. Further information on research design is available in the Nature Research Reporting Summary linked to this article.

Data availability

All datasets used in this study are publicly available from the referenced sources.

Code availability

The source code for the Bayesian DLM usedto identify the EWS is available at https://github.com/YanlanLiu/early-warning-signal-DLM.

References

50. *Landsat 7 ETM+ Surface Reflectance* (US Geological Survey, accessed 21 July 2017); https://landsat.usgs.gov/landsat-surface-reflectance-data-products
51. Hansen, M. C. et al. High-resolution global maps of 21st-century forest cover change. *Science* **342**, 850–853 (2013).
52. *MODIS Active Fire Detections for the CONUS (2002–2015)* (US Forest Service, accessed 13 September 2017); https://fsapps.nwcg.gov/afm/gisdata.php
53. Thornton, P. et al. *Daymet: Daily Surface Weather Data on a 1-km Grid for North America Version 3* (Oak Ridge National Laboratory, accessed 15 September 2017); https://doi.org/10.3334/ORNLDAAC/1328
54. Abatzoglou, J. T. Development of gridded surface meteorological data for ecological applications and modelling. *Int. J. Climatol.* **33**, 121–131 (2013).
55. *GNN Structure (Species-Size) Maps* (LEMMA Group, accessed 4 December 2017); http://lemma.forestry.oregonstate.edu/data/structure-maps
56. *Existing Vegetation–CALVEG* (US Forest Service, accessed 7 October 2017); https://www.fs.usda.gov/main/r5/landmanagement/gis
57. West, M. & Harrison, J. *Bayesian Forecasting and Dynamic Models* (Springer, 1997).
58. Finley, A., Banerjee, S. & Gelfand, A. spBayes for large univariate and multivariate point–referenced spatio-temporal data models. *J. Stat. Softw.* **63**, 1–28 (2015).
59. R Core Team *R Version 3.4.3: A Language and Environment for Statistical Computing* (R Foundation for Statistical Computing, 2017).
60. Gelfand, A. E., Banerjee, S. & Gamerman, D. Spatial process modelling for univariate and multivariate dynamic spatial data. *Environmetrics* **16**, 465–479 (2005).
61. Gelman, A., Goodrich, B., Gabry, J. & Vehtari, A. R-squared for Bayesian regression models. *Am. Stat.* **73**, 307–309 (2018).

nature research

Corresponding author(s): Mukesh Kumar

Last updated by author(s): Aug 13, 2019

Reporting Summary

Nature Research wishes to improve the reproducibility of the work that we publish. This form provides structure for consistency and transparency in reporting. For further information on Nature Research policies, see Authors & Referees and the Editorial Policy Checklist.

Statistics

For all statistical analyses, confirm that the following items are present in the figure legend, table legend, main text, or Methods section.

n/a	Confirmed	
☐	☒	The exact sample size (*n*) for each experimental group/condition, given as a discrete number and unit of measurement
☒	☐	A statement on whether measurements were taken from distinct samples or whether the same sample was measured repeatedly
☐	☒	The statistical test(s) used AND whether they are one- or two-sided *Only common tests should be described solely by name; describe more complex techniques in the Methods section.*
☐	☒	A description of all covariates tested
☐	☒	A description of any assumptions or corrections, such as tests of normality and adjustment for multiple comparisons
☐	☒	A full description of the statistical parameters including central tendency (e.g. means) or other basic estimates (e.g. regression coefficient) AND variation (e.g. standard deviation) or associated estimates of uncertainty (e.g. confidence intervals)
☐	☒	For null hypothesis testing, the test statistic (e.g. *F*, *t*, *r*) with confidence intervals, effect sizes, degrees of freedom and *P* value noted *Give P values as exact values whenever suitable.*
☐	☒	For Bayesian analysis, information on the choice of priors and Markov chain Monte Carlo settings
☒	☐	For hierarchical and complex designs, identification of the appropriate level for tests and full reporting of outcomes
☒	☐	Estimates of effect sizes (e.g. Cohen's *d*, Pearson's *r*), indicating how they were calculated

Our web collection on statistics for biologists contains articles on many of the points above.

Software and code

Policy information about availability of computer code

Data collection	Google Earth Engine was used to export Landsat 7 ETM+ surface reflectance and Daymet V3 data. Other datasets are downloadable from the original sources.
Data analysis	The software of "spBayes" in R was used for spatial analysis. An example script is publicly available at https://github.com/YanlanLiu/spatial_analysis/. A dynamic linear model (DLM) has been developed in this study and is publicly available at https://github.com/YanlanLiu/early-warning-signal-DLM/.

For manuscripts utilizing custom algorithms or software that are central to the research but not yet described in published literature, software must be made available to editors/reviewers. We strongly encourage code deposition in a community repository (e.g. GitHub). See the Nature Research guidelines for submitting code & software for further information.

Data

Policy information about availability of data

All manuscripts must include a data availability statement. This statement should provide the following information, where applicable:

- Accession codes, unique identifiers, or web links for publicly available datasets
- A list of figures that have associated raw data
- A description of any restrictions on data availability

The aerial forest survey maps are available at https://www.fs.usda.gov/detail/r5/forest-grasslandhealth/?cid=fsbdev3_046696. Landsat 7 ETM+ surface reflectance product is available at https://landsat.usgs.gov/landsat-surface-reflectance-data-products. Tree cover map is available at http://earthenginepartners.appspot.com/science-2013-global-forest. MODIS active fire product is available at https://fsapps.nwcg.gov/afm/gisdata.php. Daymet V3 climate data is available at https://daac.ornl.gov/cgi-bin/dsviewer.pl?ds_id=1328. GNN structure (species-size) map is available at https://lemma.forestry.oregonstate.edu/data/structure-maps. Existing vegetation map is available at https://www.fs.usda.gov/main/r5/landmanagement/gis.

Field-specific reporting

Please select the one below that is the best fit for your research. If you are not sure, read the appropriate sections before making your selection.

☐ Life sciences ☐ Behavioural & social sciences ☒ Ecological, evolutionary & environmental sciences

For a reference copy of the document with all sections, see nature.com/documents/nr-reporting-summary-flat.pdf

Ecological, evolutionary & environmental sciences study design

All studies must disclose on these points even when the disclosure is negative.

Study description	This study proposes to use the temporal loss of resilience, a phenomenon often detected as a system approaches a tipping point, as an early warning signal (EWS) to predict the potential for forest mortality. An application of the proposed approach using remotely sensed images of vegetation dynamics in California forests indicates that EWS can often be detected prior to reduced greenness, between 6 to 19 months prior to mortality. The EWS shows species-specific relation with mortality, and is able to capture its spatial-temporal variations. The results highlight EWS's potential for operational monitoring and near-term prediction of forest mortality.
Research sample	The study uses existing dataset to identify EWS and analyze the predictability for mortality. The datasets and the corresponding sources include the following. The aerial forest survey maps are available at https://www.fs.usda.gov/detail/r5/forest-grasslandhealth/?cid=fsbdev3_046696. Landsat 7 ETM+ surface reflectance product is available at https://landsat.usgs.gov/landsat-surface-reflectance-data-products. Tree cover map is available at http://earthenginepartners.appspot.com/science-2013-global-forest. MODIS active fire product is available at https://fsapps.nwcg.gov/afm/gisdata.php. Daymet V3 climate data is available at https://daac.ornl.gov/cgi-bin/dsviewer.pl?ds_id=1328. GNN structure (species-size) map is available at https://lemma.forestry.oregonstate.edu/data/structure-maps. Existing vegetation map is available at https://www.fs.usda.gov/main/r5/landmanagement/gis.
Sampling strategy	No sampling strategy is involved.
Data collection	Existing datasets are downloaded from the sources indicated above.
Timing and spatial scale	The Landsat 7 and Daymet3 data used for the analyses range from 1999 to 2015. The available aerial survey data from 2005 to 2015 are used. The datasets cover the forested area within the state of California, USA.
Data exclusions	As described in the methods, data points affected by fire and human activities are excluded from the analysis. These data points are outside the scope of the study on detecting climate-induced reduction of resilience.
Reproducibility	Results can be reproduced using existing datasets and the code/software used. Attempts to repeat the analyses were successfull.
Randomization	No randomization is involved.
Blinding	Theoretical analysis, alternative model analysis, examination on alternative explanations, and sensitivity analysis are performed and described in the supporting information. These analysis support the robustness of the findings in this study.

Did the study involve field work? ☐ Yes ☒ No

Reporting for specific materials, systems and methods

We require information from authors about some types of materials, experimental systems and methods used in many studies. Here, indicate whether each material, system or method listed is relevant to your study. If you are not sure if a list item applies to your research, read the appropriate section before selecting a response.

Materials & experimental systems

n/a	Involved in the study
☒	☐ Antibodies
☒	☐ Eukaryotic cell lines
☒	☐ Palaeontology
☒	☐ Animals and other organisms
☒	☐ Human research participants
☒	☐ Clinical data

Methods

n/a	Involved in the study
☒	☐ ChIP-seq
☒	☐ Flow cytometry
☒	☐ MRI-based neuroimaging